Electromagnetic Analysis of Plane Wave Illumination Effects Onto Passive and Active Circuit Topologies

E. S. Siah, J. L. Volakis, *Fellow, IEEE,* D. Pavlidis, *Fellow, IEEE*, and V. V. Liepa, *Life Member, IEEE*

***Abstract*—In this letter, the finite element-boundary integral method, incorporating the multilevel fast multipole method to reduce the storage cost of the boundary integral matrix, is applied to the analysis of two microstrip filter circuits illuminated via a plane wave. Simulated results indicate that significant voltages are induced across the output ports close to filters' resonances. This study is further extended to a microstrip low-noise amplifier circuit. It will be shown that at certain field strengths, the plane wave illuminating the microstrip amplifier circuit can introduce considerable gain deviation and nonlinearity to its operation.**

***Index Terms*—Boundary integral, electromagnetic compatibility/interference (EMC/EMI), finite element, harmonic balance method, method of moments (MoM).**

I. Introduction

With the uptake of wireless devices and services, the impact of electromagnetic (EM) coupling and interference on active circuits exposed to ambient radiation is of increasing concern. This interference can be intentional or unintentional and could result in a distortion of the output signal for analog devices and in digital circuit logic errors leading to improper functionality of digital systems. In recent years, various numerical tools such as the method of moments (MoM), the finite-element method (FEM), and the finite-difference time-domain (FDTD) method have been applied to the analysis of electromagnetic compatibility (EMC) and electromagnetic interference (EMI) problems. Of particular interest is the use of the MoM coupled with the multilevel fast multipole method to the analysis of complicated structures resulting in O(NlogN) computation cost. In this letter, we employ the hybrid finite element-boundary integral (FE-BI) method for the analysis of EM coupling from an external plane wave on two passive circuit elements (a microstrip interdigital filter and a coupled microstrip line filter). Also, an external plane wave is used to illuminate the peripheral circuitry of a low-noise amplifier (LNA) circuit to generate the induced voltages at the gate and the drain terminals of the LNA. These input voltages are modeled as extraneous sources in conjunction with the harmonic balance method to evaluate the distortions on the gain and the degree of nonlinearities introduced on the LNA by external coupling. It is shown that significant interference on the device operation can be caused by this excitation. To the authors' knowledge, this is the first time full wave methods have been used to evaluate the influence of external EM interference on the performance of an active circuit. It is worthwhile to note that in [7], the authors have utilized time-domain integral equations in the analysis of idealized perfectly electrical conductor (PEC) motherboard geometries.

Manuscript received April 29, 2003; revised August 26, 2003. This work was supported by U.S. Air Force MURI Grant F49620–01-1–0436.

E. S. Siah, D. Pavlidis, and V. V. Liepa are with the Department of Electrical Engineering and Computer Science, University of Michigan, Ann Arbor, MI 48109-2122 USA (e-mail: esiah@eecs.umich.edu; pavlidis@eecs.umich.edu).

J. L. Volakis is with the Department of Electrical Engineering and Computer Science, University of Michigan, Ann Arbor, MI 48109-2122 USA, and also with the ElectroScience Laboratory, Ohio State University, Columbus, OH 43210 USA (e-mail: volakis@eecs.umich.edu).

Digital Object Identifier 10.1109/LAWP.2003.819691

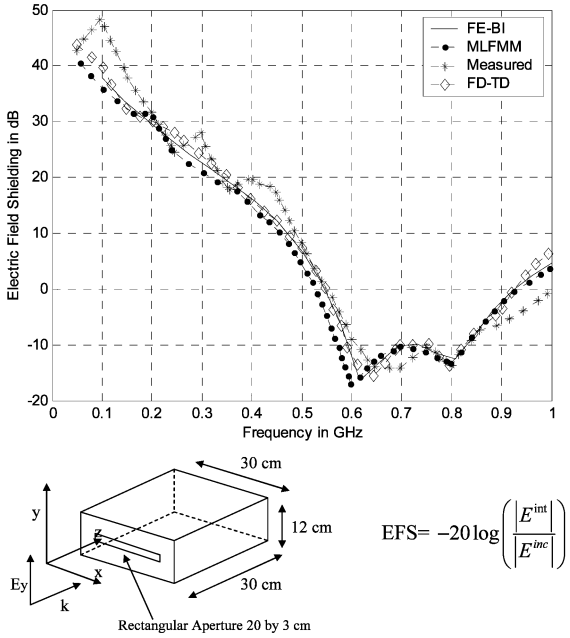

Fig. 1. Validation of the FE-BI method for computing the electric field shielding (EFS).

II. Validation of Analysis Method

The pertinent analysis method used for our analysis in this letter is the FE-BI method. This approach is a hybridization of the FEM used to model the interior volume of the geometry and the moment method for modeling the fields on the geometry boundary [1]–[3]. The employed FE-BI approach utilizes curvilinear hexahedral rooftop basis functions and curvilinear bi-quadratic rooftop functions for surface modeling [4]. Also, the multilevel fast mutlipole method (MLFMM) is incorporated for the fast implementation of the matrix–vector product associated with the boundary integral portion of the FE-BI system matrix [5]. A pertinent validation example for the FE-BI method and the associated code used here is given in Fig. 1, where the electric field is computed at the center of the enclosed cavity. The cavity is perforated with an aperture and the excitation is a plane wave polarized in the y direction, incident normal to the

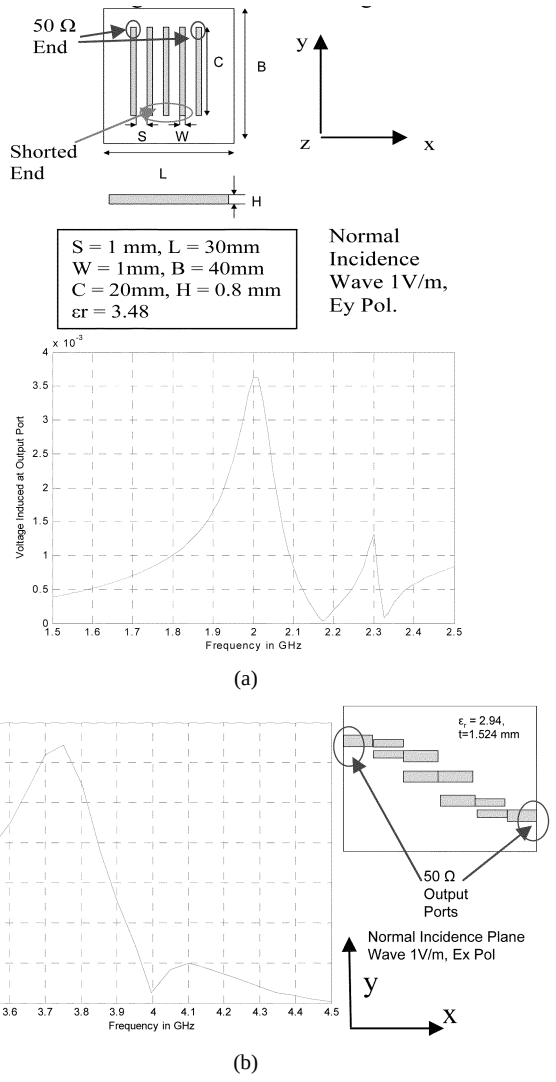

Fig. 2. (a) Induced voltages at the 50 Ω ports due to plane wave illumination at normal incidence to the substrate for an interdigital microstrip filter. (b) Induced voltages at the 50 Ω ports due to plane wave illumination at normal incidence to the substrate for a coupled line microstrip filter.

aperture. The FE-BI computed EFS (defined in Fig. 1) shows excellent agreement with both measured and reference simulations based on FDTD [6] and MoM accelerated by MLFMM. Details of the relevant formulation of our FE-BI method are given in the Appendix.

III. Simulation Results

To quantitatively evaluate coupling effects from external sources on passive devices, we consider two microwave devices shown in Fig. 2(a) and (b). These refer to a microstrip interdigital filter and a coupled microstrip line filter. These filters are subjected to an external plane wave illumination with a spectrum wider than their operational bandwidth. For this computation, the output and input ports are terminated with 50 Ω loads and the induced voltages (analyzed with the FE-BI method) are computed across these ports. With the incident plane wave intensity at 1 V/m [and polarization defined in Fig. 2(a) and (b)], we observe an induced voltage of 3.65 mV and 13 mV at the outputs of the interdigital and the coupled microstripline filter, respectively. These values refer to the

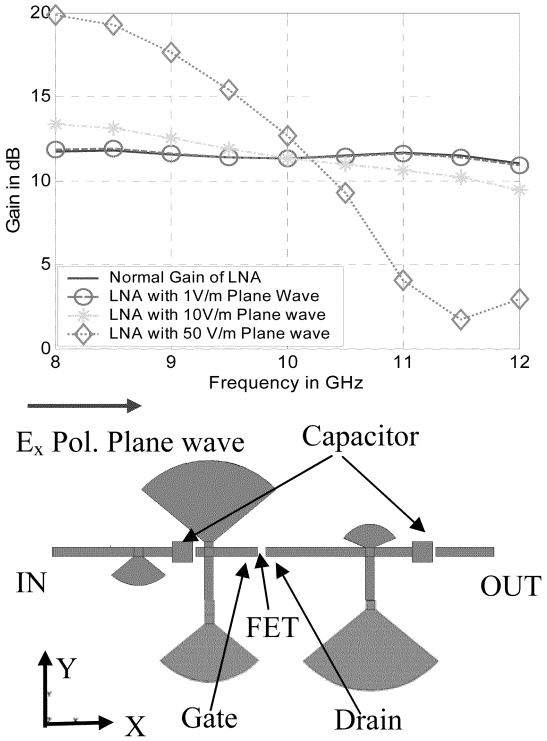

Fig. 3. Gain variations due to the plane wave illumination onto the substrate of the low noise amplifier circuit.

peaks of the response curves shown in Fig. 2(a) and (b) and, as expected, occur close to the designed resonance of the microwave filter circuits. Clearly, such coupling distortions can be significant for excitations with rather large field strengths. Specifically, if an excitation of 100 V/m is considered, the maximum output voltages rises to 0.365 and 1.3 V, respectively. These are significantly high to cause logic state errors and distortion at both the input and output terminals of digital devices and analog circuits respectively.

The above analytical study was next applied to the analysis of a low noise amplifier operating with a gain of 11 to 12 dB from 8 to 12 GHz. For this analysis, the dimensions of the field effect transistor (FET) metal regions are much smaller than a wavelength. Thus, the input impedances looking into the gate and drain terminals of the FET can be modeled as lumped loads attached to the respective terminals of the LNA. These load values varies with frequency depending upon the FET characteristics and geometry of the circuit at the opposite port. The geometry of the LNA is shown in the operational bandwidth of the LNA were considered. In this example, the LNA is on a substrate with a permittivity of 9.7 and uses a Gallium Nitrite (GaN) high electron mobility transistor (HEMT) device. The gain of the LNA is defined as the ratio of the voltage at the output port and the input ports, with the latter fixed at 10 mV. Fig. 3 and, in this case, a plane wave, illuminates the entire circuit at normal incidence. For our study, an x-polarized wave was assumed for excitation and various amplitude levels within the operational bandwidth of the LNA were considered. In this example, the LNA is on a substrate with a permittivity of 9.7 and uses a GaN HEMT device. The gain of the LNA is defined as the ratio of the voltage at the output port and the input ports (input fixed at 10 mV).

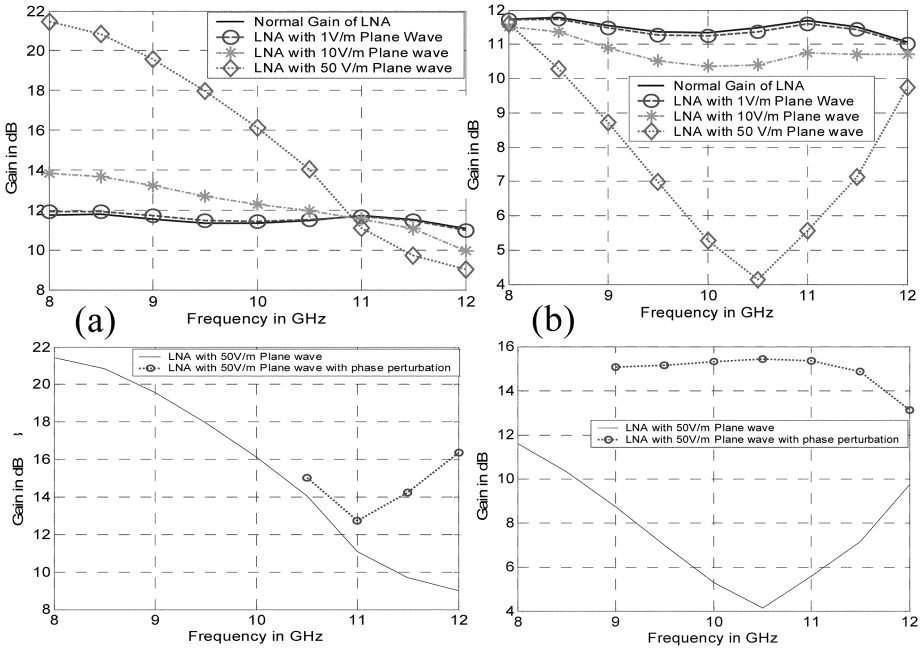

Fig. 4. Gain with induced voltages at the (a) gate only and at the (b) drain only. Also in this figure, gain with random phase perturbations introduced to the induced gate voltages (a) and to the induced drain voltages is shown.

Induced voltages at the gate and drain terminals of the HEMT are first computed with the FE-BI method under plane wave illumination. Next, these voltages are modeled as extraneous sources in a single tone harmonic balance simulation to evaluate its effect on the LNA performance. The values of input driving voltages and amplitudes of the external plane wave were implicitly chosen such that the HEMT operates within the linear region, which is typical of most LNA devices. As the amplitude of the plane wave is increased, the LNA gain distortion is increased (Fig. 3).

Specifically, our analysis shows that as the plane wave intensity is increased, the LNA gain is increased at lower frequencies and subsequently decreases as frequency is increased. This gain deviation is explained in Fig. 4, where the induced gate and drain voltages are modeled separately. In this study, either one of the induced gate or drain voltages is used with the other neglected. This allows the effect of each induced voltage on the LNA performance to be analyzed. In Fig. 4, a similar distortion in the LNA gain is observed when the amplitude of the plane wave increases throughout the frequency range. However, a phase perturbation either at the induced gate or drain voltages resulted in a significant increase in the LNA's gain. This observation allows us to assert that the decrease in LNA gain at higher frequencies is not due to saturation of the HEMT. Instead, the deviation of the LNA gain from the designed gain is due to coherent addition or subtraction of the voltage signals at the gate and the drain terminals of the HEMT. When this LNA is connected to digital circuits, such EM interference may result in bit errors at the output terminal, leading to improper functionality and change of the device logic state.

A study on the degree of nonlinearity introduced to the LNA circuit is performed next. In this study, the LNA operates at 10 GHz (f_1) while, at the same time, a 9.5 GHz (f_2) external plane wave with the same orientation and polarization as before illuminates the LNA circuit. Similar to above, the induced voltages are computed at the gate and drain terminals of the HEMT at frequency f_2. These voltages are in turn modeled as extraneous voltage sources with the LNA operating at f_1. A two-tone harmonic balance simulation using these induced voltage sources allows one to examine the third harmonic content (IP3) of the LNA circuit. Ideally, this should be zero for a linear amplifier in the absence of ambient radiation. The IP3 simulation is shown in Fig. 5 where we compare the LNA output power at the fundamental (f_1) and the third harmonic ($2f_1 - f_2$) for various input power levels. The incident plane wave amplitude was kept at 50 V/m. As seen from Fig. 5, the introduction of high-power plane wave illumination lead to significant nonlinearities in the LNA circuit, which now exhibits a third order inter-modulation product of 40 dBm. In addition, the third-order harmonic content for the LNA under illumination is now significantly higher compared to the LNA operating in isolation. That is, the external illumination introduces significant nonlinearities as compared to an isolated (hardened) device.

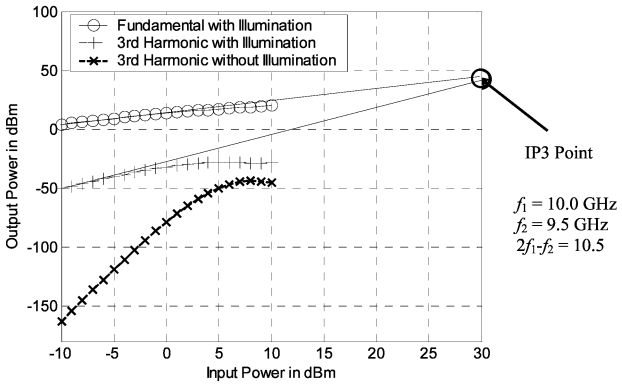

Fig. 5. Diagram showing the introduction of nonlinearity into the low-noise amplifier circuit operating at 10 GHz with plane wave illumination at 9.5 GHz.

IV. Conclusion

We applied the hybrid FE-BI method to the analysis of ambient radiation onto passive and active circuit topologies. The simulated results indicate that passive microstrip interdigital and coupled microstripline filters could exhibit significant induced voltages at frequencies close to their designed resonances. When such peripheral circuits are connected to active devices such as amplifiers and oscillators, significant nonlinearities, and gain deviations are introduced. This can have an effect on the entire device performance and can furthermore cause logic errors when digital circuits are considered.

Appendix

In the formulation of the FE-BI incorporating curvilinear hexahedral elements, the fields within a volumetric domain is solved by setting $\partial \mathrm{F}(\mathbf{E})/\partial \mathbf{E} = 0$, where the function $\mathrm{F}(\mathbf{E})$ is

$$F(E) = \frac{1}{2}\int_v [(\nabla \times E)\cdot \bar{\mu}_r^{-1}\cdot(\nabla \times E) - k_0^2 E\cdot\bar{\varepsilon}_r\cdot E]dr - ik_0\eta_0 \int_S \hat{n}\cdot(E\times H)dr \quad (1)$$

where $\bar{\mu}_r$ and $\bar{\varepsilon}_r$ are the tensor permeability and permittivity of the inhomogeneous medium, k_0 and η_0 are the wavenumber and the characteristic impedance in free space. The boundary integral is taken along the surface s bounding the volume v and the normal of this surface is taken pointing outwards from the volume v. The E field can be related to the H field by using the Stratton Chu's integral equations and, upon discretizing (1), leads to

$$\begin{bmatrix} E_{vv} & E_{vs} & 0 \\ E_{sv} & E_{ss} & B \\ 0 & P & Q \end{bmatrix}\begin{bmatrix} E_v \\ E_s \\ H_s \end{bmatrix} = \begin{bmatrix} b_i \\ b_s \\ b_e \end{bmatrix} \quad (2)$$

$$E_{ji} = \int_v dr \nabla\times e_j\cdot\bar{\mu}_r\cdot\nabla\times e_i + \int_v dr e_j\cdot\bar{\varepsilon}_r\cdot e_i \quad (3)$$

$$B_{ji} = ik_0\eta_0\int_s dr e_j\cdot(\hat{n}\times h_i) \quad (4)$$

$$P_{ji} = \int_s dr(\hat{n}\times h_j)\cdot[-\alpha\Omega(e_i\times\hat{n}) + (1-\alpha)\Theta(e_i\times\hat{n})] \quad (5)$$

$$Q_{ji} = \eta_0\int_s dr(\hat{n}\times h_j)\cdot[\alpha\Theta(\hat{n}\times h_i) + (1-\alpha)\Omega(\hat{n}\times h_i)] \quad (6)$$

$$b_e = \alpha\int_s dr(\hat{n}\times h_j)\cdot E^{inc} + (1-\alpha)\int_s dr(\hat{n}\times h_j)\cdot H^{inc} \quad (7)$$

$$\Theta(X) = ik_0\int_s dr'\bar{G}(r,r')\cdot X(r') \quad (8)$$

$$\Omega(X) = TY(r) + \int_s dr' X(r')\times\nabla g(r,r') \quad (9)$$

where $\mathrm{T} = 1-\beta/4\pi$ and $X = \hat{n}\times Y$. The parameter α indicates the combined field integral equation (CFIE) factor, chosen from zero to unity. The vector E_v refers to the electric fields within the volume of the geometry while the vectors E_s and H_s refer to the fields along the surface of the boundary and b_i, b_s denotes internal port or antenna feeds

$$r(u,v,w) = \sum_{i=0}^{2}\sum_{j=0}^{2}\sum_{k=0}^{2} L_{ijk}(u,v,w)r_{ijk} \quad (10)$$

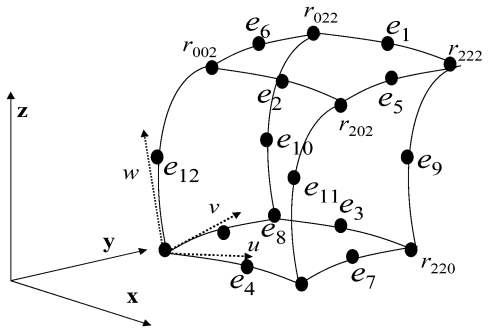

Fig. 6. Geometry of a curvilinear hexahedral element.

$$a_u = \frac{\partial r}{\partial u} \quad av = \frac{\partial r}{\partial v} \quad a_w = \frac{\partial r}{\partial w} \quad (11)$$

$$a^u = \frac{1}{V_+}(a_v\times a_w)\; a^v = \frac{1}{V_+}(a_w\times a_u) \quad (12)$$

$$a^w = \frac{1}{V_+}(a_u\times a_v)\; V_+ = a_u\cdot(a_v\times a_w). \quad (13)$$

The basis and testing functions are chosen as the 12 edges of the curvilinear hexahedral element (Fig. 6). The representation of each of the 27 points in u, v and w space is given in (10) and the covariant and contravariant notaions are given in (11)–(13). Each of the 12 basis and testing functions are thus given as

$$\begin{aligned} e_1 &= vwa^u\; e_2 = (1-v)wa^u\; e_5 = uwa^v\; e_9 = uva^w \\ e_3 &= v(1-w)a^u\; e_4 = (1-v)(1-w)a^u\; e_7 = u(1-w)a^v \\ e_6 &= (1-u)wa^v\; e_8 = (1-u)(1-w)a^v\; e_{10} = (1-u)va^w \\ e_{11} &= u(1-v)a^w\; e_{12} = (1-u)(1-v)a^w. \end{aligned}$$

Acknowledgment

The authors would like to thank Dr. K. Sertel and Mr. R. Kindt for their help in the course of this work.

References

[1] T. Eibert and J. L. Volakis, "Fast spectral domain algorithm for hybrid finite element/boundary integral modeling of doubly periodic structures," *Inst. Elect. Eng. Proc. Microwaves, Antennas, Propagat.*, vol. 147, no. 5, pp. 329–334, Oct. 2000.

[2] T. F. Eibert, K. Sertel, and J. L. Volakis, "Hybrid finite element modeling of conformal antenna and array structures utilizing fast integral methods," *Int. J. Numer. Modelling: Electron. Networks Devices Fields*, vol. 13, pp. 2–3, Mar.–June 2000.

[3] J. L. Volakis, A. Chatterjee, and L. Kempel, *Finite Element Methods for Electromagnetics*. New York: IEEE Press, 1998.

[4] K. Sertel and L. Gurel, "A comparison of surface modeling techniques," in *Proc. IEEE Antennas and Propagation Soc. Conf. Dig.*, vol. 3, 1997, pp. 1834–1837.

[5] X. Q. Sheng, J. J. Jin, J. Song, C. Lu, and W. C. Chew, "On the formulation of hybrid finite-element and boundary-integral methods for 3-D scattering," *IEEE Trans. Antennas Propagat.*, vol. 46, pp. 303–311, Mar. 1998.

[6] M. P. Robinson, T. M. Benson, C. Christopoulos, J. F. Dawson, M. D. Ganley, A. C. Marvin, S. J. Porter, and D. W. P. Thomas, "Analytical formulation for the shielding effectiveness of enclosures with apertures," *IEEE Trans. Electromagn. Compat.*, vol. 40, pp. 240–248, Aug. 1998.

[7] K. Aygün, B. Shanker, A. A. Ergin, and E. Michielssen, "A two-level plane wave time-domain algorithm for fast analysis of EMC/EMI problems," *IEEE Trans. Electromagn. Compat.*, vol. 44, pp. 152–163, Feb. 2002.